Title	On nonlinear multiarmed spiral waves in slowly rotating systems
Author(s)	Li, L; Liao, X; Chan, KH; Zhang, K
Citation	Physics of Fluids, 2010, v. 22 n. 1, p. 011701
Issued Date	2010
URL	http://hdl.handle.net/10722/65461
Rights	Physics of Fluids. Copyright © American Institute of Physics.

On nonlinear multiarmed spiral waves in slowly rotating fluid systems

Ligang Li,[1] Xinhao Liao,[1] Kit H. Chan,[2] and Keke Zhang[3]
[1]*Shanghai Astronomical Observatory, Chinese Academy of Sciences, Shanghai 200030, China*
[2]*Department of Mathematics, The University of Hong Kong, Pokfulam, Hong Kong*
[3]*Department of Mathematical Sciences, University of Exeter, Exeter EX4 4QE, United Kingdom*

(Received 28 August 2009; accepted 13 November 2009; published online 7 January 2010)

Stable nonlinear equilibria of convection in the form of quasistationary, multiarmed spiral waves, up to a maximum of six spiral arms, are found in a slowly rotating fluid confined within a thin spherical shell governed by the three-dimensional Navier–Stokes equation, driven by a radial unstable temperature gradient and affected by a weak Coriolis force. It is shown that three essential ingredients are generally required for the formation of the multiarmed spirals: the influence of slow rotation, large-aspect-ratio geometry and the effect of weak nonlinearity. © *2010 American Institute of Physics*. [doi:10.1063/1.3276277]

On a large scale, quasistationary giant multiarmed spirals are observed in a rotating galaxy.[1] In a small-scale excitable medium, it is also known that multiarmed spirals take place in a variety of physical, chemical, and biological systems (e.g., Refs. 2–4). The FitzHugh–Nagumo equations, two coupled model equations, have been widely and successfully employed to describe the formation of multiarmed spirals in a prototype excitable medium (e.g., Ref. 5). The formation of nonlinear long-extended multiarmed spirals in slowly rotating self-gravitating spherical systems that are governed by the three-dimensional (3D) Navier–Stokes equations with the Coriolis force and maintained by convective instabilities is less well studied and understood. This letter reports the finding of quasistationary, multiarmed spiral waves, up to a maximum of six spiral arms, which occur as a stable nonlinear equilibrium bifurcating from a slowly rotating, self-gravitating spherically symmetric state, driven by a radial unstable temperature gradient. The configuration of the problem is approximately realizable in laboratory experiments[6] and relevant to many astrophysical fluid systems.[7]

We consider a Boussinesq fluid confined in a spherical shell of inner radius r_i and outer radius r_o with constant thermal diffusivity κ, thermal expansion coefficient α, and kinematic viscosity ν. The fluid spherical shell rotates slowly with a constant angular velocity $\mathbf{\Omega}$ in the presence of its own gravitational field $-\gamma\mathbf{r}$ along with an unstable temperature gradient $-\beta\mathbf{r}$, where γ and β are positive constants and $\mathbf{r}$ is the position vector. The convection problem is governed by the dimensionless equations

$$\frac{\partial \mathbf{u}}{\partial t} + \mathbf{u}\cdot\nabla\mathbf{u} + \mathrm{Ta}^{1/2}\mathbf{k}\times\mathbf{u} = -\nabla p + R\Theta\mathbf{r} + \nabla^2\mathbf{u}, \tag{1}$$

$$\mathrm{Pr}\left(\frac{\partial \Theta}{\partial t} + \mathbf{u}\cdot\nabla\Theta\right) = \mathbf{u}\cdot\mathbf{r} + \nabla^2\Theta, \tag{2}$$

$$\nabla\cdot\mathbf{u} = 0, \tag{3}$$

where $\mathbf{k}$ is a unit vector parallel to the axis of rotation, Θ, which is associated with density variation, denotes temperature perturbation from the basic spherically symmetric state, p is the total pressure, and $\mathbf{u}$ is the 3D velocity field, $\mathbf{u}=(u_r,u_\theta,u_\phi)$ in spherical polar coordinates (r,θ,ϕ) with $\theta=0$ at the axis of rotation. Three nondimensional parameters, the Rayleigh number R, the Prandtl number Pr, and the Taylor number Ta, are defined as $R=\alpha\beta\gamma(r_o-r_i)^4/\nu\kappa$, $\mathrm{Pr}=\nu/\kappa$, $\mathrm{Ta}=[2\Omega(r_o-r_i)^2/\nu]^2$. Additionally, there is a geometrical parameter, the aspect ratio $\Gamma=r_o/(r_o-r_i)$. The velocity boundary conditions assumed are nonslip and constant temperature, which yields $u_r=u_\theta=u_\phi=\Theta=0$ at the bounding surfaces $r=r_i,r_o$. We shall carry out both linear and nonlinear analysis of Eqs. (1)–(3) to demonstrate that giant multiarmed spirals cannot occur in linear systems while they are naturally formed in weakly nonlinear systems at moderately supercritical Rayleigh numbers.

It is insightful to look at the linear problem before revealing the nonlinear multiarmed spirals. In the linear analysis, we expand the velocity $\mathbf{u}$ as a sum of poloidal (v) and toroidal vectors (w) in the form

$$\mathbf{u} = [\nabla\times\nabla\times\mathbf{r}v(r,\theta,\phi) + \nabla\times\mathbf{r}w(r,\theta,\phi)]e^{i\omega t}, \tag{4}$$

where (r,θ,ϕ) are spherical polar coordinates and ω is the frequency of a wave. Making use of the expansion (4), we can derive three independent scalar equations from the linearized equations (1)–(3)

$$0 = \left(\nabla^2\mathcal{L} + \mathrm{Ta}^{1/2}\frac{\partial}{\partial\phi} - i\omega\mathcal{L}\right)\nabla^2 v + \mathrm{Ta}^{1/2}\mathcal{Q}w - R\mathcal{L}\Theta, \tag{5}$$

$$0 = \left(\nabla^2\mathcal{L} + \mathrm{Ta}^{1/2}\frac{\partial}{\partial\phi} - i\omega\mathcal{L}\right)w - \mathrm{Ta}^{1/2}\mathcal{Q}v, \tag{6}$$

$$0 = (\nabla^2 - i\omega\mathrm{Pr})\Theta + \mathcal{L}v, \tag{7}$$

where the differential operators $\mathcal{L}$ and $\mathcal{Q}$ are defined as

$$\mathcal{L} = -r^2\nabla^2 + \frac{\partial}{\partial r}r^2\frac{\partial}{\partial r}, \quad \mathcal{Q} = \mathbf{k}\cdot\nabla - \frac{1}{2}(\mathcal{L}\mathbf{k}\cdot\nabla + \mathbf{k}\cdot\nabla\mathcal{L}).$$

The boundary conditions for v, w, and Θ become $v=\partial v/\partial r=w=\Theta=0$ at $r=r_i,r_o$. Equations (5)–(7) are then solved

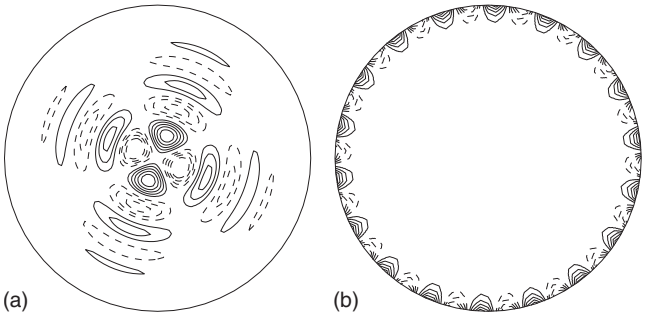

FIG. 1. Temperature Θ, linear solutions to Eqs. (5)–(7) are obtained for Ta=100 and Pr=7.0 with Γ=6.556: (a) for the polar mode with m=2 and (b) the equatorial mode with m=18.

by expanding the velocity potentials and temperature in terms of spherical harmonics, for example, $\Theta=[\Sigma_{l,n}\Theta_{ln}(r)P_l^m(\cos\theta)]e^{i(m\phi)}$, where $P_l^m(\cos\theta)e^{im\phi}$ denotes the standard spherical harmonics of degree l normalized by $\int_0^{2\pi}\int_0^{\pi}|P_l^m(\cos\theta)e^{im\phi}|^2\sin\theta\mathrm{d}\theta\mathrm{d}\phi=4\pi$, and $\Theta_{ln}(r)$ satisfies the relevant boundary condition. The aim of the linear analysis is, for a given m, Ta, and Pr to find v, w, Θ, and R satisfying Eqs. (5)–(7) such that ω is real; the numerical method of the linear analysis was discussed, for example, in detail by Ref. 8. Both the linear and nonlinear analyses will focus on a large aspect ratio with Γ=6.556.

While the properties of Eqs. (5)–(7) in rapidly rotating systems are well studied and understood (e.g., Refs. 9–12), the dynamics and physics in slowly rotating systems with large aspect ratio $\Gamma\gg1$ are quite different. Our extensive calculation indicates that there exist two different types of linear solution: polar modes and equatorial modes. The typical profile of Θ describing the polar mode at the middle surface of the shell obtained for m=2, R=48.48, $\omega=3.558\times10^{-3}$ with Ta=100, Pr=7 is depicted in Fig. 1(a), while the equatorial mode for m=18, R=46.76, $\omega=3.513\times10^{-2}$ also with Ta=100, Pr=7 is displayed in Fig. 1(b). Both the polar and equatorial modes are approximately represented by the combination of three spherical harmonics, $P_l^m(\cos\theta)e^{im\phi}$, $P_{l-2}^m(\cos\theta)e^{im\phi}$, and $P_{l+2}^m(\cos\theta)e^{im\phi}$, which are coupled together by a weak effect of rotation but have an insignificant phase difference between them. For moderate values of Ta, our linear analysis reveals that the Rayleigh number for the onset of the polar modes is always slightly larger than that for the equatorial modes. For the case of Ta=100 and Pr=7, the critical Rayleigh number R_c at the onset of convection is given by R_c=46.76. A major conclusion is that multiarmed spiral waves cannot be formed in slowly rotating linear systems.

For thin-shell geometry, it is numerically efficient to tackle the nonlinear problem by using a second-order finite-difference method based on the Chorin-type projection scheme,[13] which decouples the momentum and continuity equations through a predictor-corrector procedure. The projection scheme leads to the time discretization of Eqs. (1)–(3) in the form

$$\frac{\tilde{\mathbf{u}}-\hat{\mathbf{u}}}{\Delta t}=R\mathbf{r}\left(\frac{\Theta^n+\Theta^{n+1}}{2}\right)-\mathrm{Ta}^{1/2}\mathbf{k}\times\left(\frac{\tilde{\mathbf{u}}+\hat{\mathbf{u}}}{2}\right)+\nabla^2\left(\frac{\tilde{\mathbf{u}}+\hat{\mathbf{u}}}{2}\right)-(\mathbf{u}\cdot\nabla\mathbf{u})^{n+1/2},\tag{8}$$

$$\frac{\Theta^{n+1}-\Theta^n}{\Delta t}=\frac{\mathbf{r}}{\mathrm{Pr}}\cdot\left(\frac{\tilde{\mathbf{u}}+\hat{\mathbf{u}}}{2}\right)+\frac{1}{\mathrm{Pr}}\nabla^2\left(\frac{\Theta^n+\Theta^{n+1}}{2}\right)-(\mathbf{u}\cdot\nabla\Theta)^{n+1/2},\tag{9}$$

where $\mathbf{u}^n$ and Θ^n represent the velocity and temperature, respectively, at the nth time step $t=t_n$, $\hat{\mathbf{u}}=\mathbf{u}^n-(\Delta t/2)\nabla p^n$, $\tilde{\mathbf{u}}$ denotes the velocity at an intermediate time between $t=t^n$ and $t=t^{n+1}$ and the second-order Adams–Bashforth formula is used for the nonlinear terms. For given $(\mathbf{u}^{n-1},\Theta^{n-1})$ and $(\mathbf{u}^n,p^n,\Theta^n)$, Eqs. (8) and (9) determine Θ^{n+1}, as well as $\tilde{\mathbf{u}}$, which is then used to solve the Poisson equation for the pressure p^{n+1}, $\nabla^2p^{n+1}=(2/\Delta t)\nabla\cdot\tilde{\mathbf{u}}$. The relationship between $\mathbf{u}^{n+1}$ and p^{n+1} at $t=t_{n+1}$ is simply given by $\mathbf{u}^{n+1}=\tilde{\mathbf{u}}-(\Delta t/2)\nabla p^{n+1}$. The validity and accuracy of our 3D nonlinear simulations are checked by calculating the numerical solutions using different spatial and temporal resolutions, by comparing with the spectral benchmark solution and with the finite element solution.[14,15] Typically, we used the spatial resolution with the number of grid points $[30\times150\times120]$ in (r,θ,ϕ) coordinates for the thin spherical shell.

At the heart of the formation of multiarmed spiral waves are the competing influences of slow rotation and weak nonlinearity in a large aspect-ratio system. We have carried out an extensive nonlinear computation over a wide range of moderate values of Ta and R with each simulation usually running up to $O(10^2)$ viscous diffusion time units to reach a final quasistationary equilibrium in which the solution remains unchanged both temporally and spatially in the frame drifting with the phase speed of the waves. Figure 2 shows six different stable nonlinear equilibria obtained for Ta=100, R=60, and Pr=7 at the aspect ratio Γ=6.556 with different initial conditions. It is found that the multiarmed giant spirals, up to a maximum of six spiral arms, are quasistationary, precessing retrogradely with constant speed, start from the common core located at the pole and terminate at the equator. The frequencies of the precessing multiarmed waves are given in Table I. To measure the strength of the multiarmed spiral waves, we introduce the kinetic energy density $E_{\mathrm{kin}}=(2V)^{-1}\int_V|\mathbf{u}|^2\mathrm{d}V$ and the Nusselt number $\mathrm{Nu}=1+(\mathrm{Pr})^2[r_i(r_o-r_i)/r_o^2]\int_V(u_r\Theta)\mathrm{d}V$, where V is the volume of the shell. They are given in Table I for the six multiarmed spirals. It can be seen that both E_{kin} and Nu for the different multiarmed spirals are quite close.

A comparison between the linear solution depicted in Fig. 1(a) for m=2 and its corresponding nonlinear two-armed spirals in Fig. 2(b) is highly revealing. The projection of the finite-difference solution onto the spherical harmonic spectrum suggests that the two-armed spirals shown in Fig. 2(b) are still dominated by the three spherical harmonics, $P_{18}^2(\cos\theta)e^{i2\phi}$, $P_{16}^2(\cos\theta)e^{i2\phi}$, and $P_{20}^2(\cos\theta)e^{i2\phi}$. However, the nonlinear effect generates the differential rotation and higher spherical harmonics (e.g., Ref. 16), which in turn

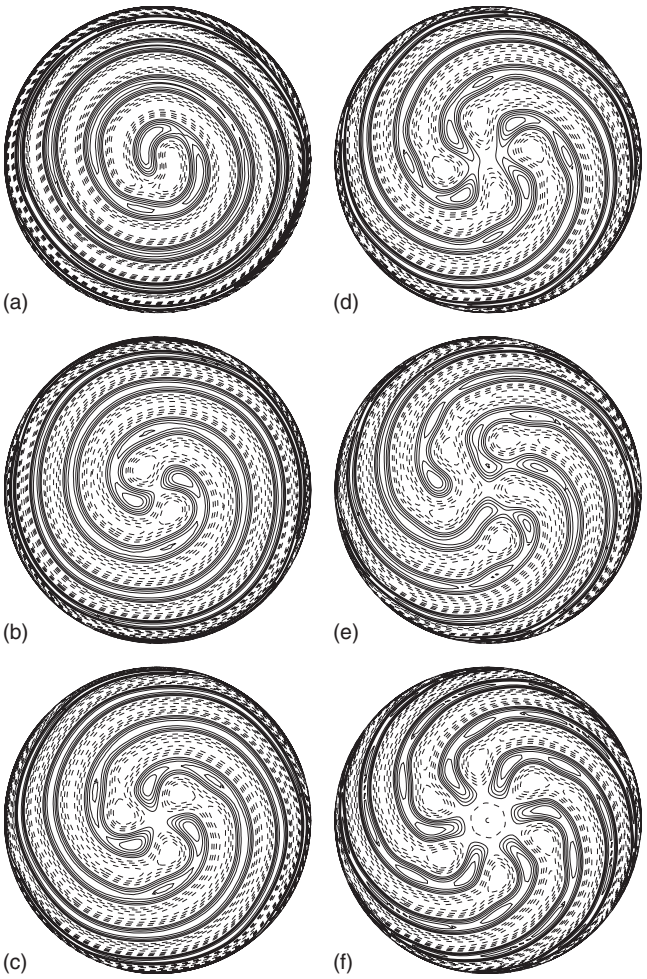

FIG. 2. Six stable nonlinear equilibria in the form of multiarmed spiral waves, showing temperature Θ viewed from the axis of rotation are obtained for Ta=100 and Pr=7.0 at $R=60$. The key characteristics of the waves are given in Table I.

change the relative phases between the three spherical harmonics and thus produce multiarmed spiral waves.

A simple model may be used to explain how and why giant multiarmed spirals can be formed. Three essential ingredients are required to produce a giant multiarmed spiral: (i) large-aspect-ratio geometry implying thin spherical shells or highly flattened spheroids, (ii) the influence of slow rotation, and (iii) the weak effect of nonlinearity. Consider first pattern formation in spherical systems without rotation,

TABLE I. The kinetic energy density E_{kin}, the Nusselt number Nu and the frequency ω of multiarmed spiral nonlinear waves for Ta=100 and Ra =60 with $\Gamma=6.556$. The corresponding structure of the waves is depicted in Fig. 2.

Number of spiral arms	E_{kin}	Nu	ω
1	0.1317	1.054	1.234×10^{-3}
2	0.1306	1.054	2.902×10^{-3}
3	0.1279	1.053	3.267×10^{-3}
4	0.1246	1.051	6.100×10^{-3}
5	0.1217	1.050	8.430×10^{-3}
6	0.1156	1.048	1.024×10^{-2}

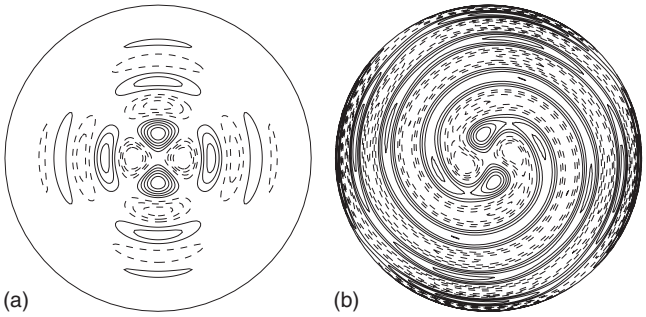

FIG. 3. The structure Θ, viewed from $\theta=0$, is computed from Eq. (11) with $m=2$, $l=18$, and $\mathcal{S}=0.34$: (a) for $\phi_1=\phi_2=0$ and (b) for $\phi_1=-2.0$, $\phi_2=1.8$.

which has been studied by a number of authors (e.g., Refs. 17–19). We know that a general 2D pattern bifurcating from a spherically symmetric state may be described by

$$\Theta(\theta,\phi)=\sum_{m=0}^{m=l} C_m P_l^m(\cos\theta)e^{im\phi}, \tag{10}$$

where m is the azimuthal wavenumber and complex coefficients $C_m, m=0,1,\ldots,l$, giving rise to $(2l+1)$-fold degeneracy, are to be determined. Note that the spherical harmonics of different l in nonrotating systems, as shown in Eq. (10), are decoupled. The size of l usually corresponds to the thickness of a spherical shell:[17] a thinner shell is typically associated with a higher degree l. A complete elimination of the $(2l+1)$-fold degeneracy by nonlinearity, particularly when $l\gg O(1)$, is a highly challenging task.[17,18] In order to form a giant multiarmed spiral, a sufficiently complex structure in the latitudinal direction, in connection with $l\gg O(1)$ or large-aspect-ratio geometry, is needed. Second, consider the effect of slow rotation on the spherical pattern. It is well understood that rotation has three major effects (e.g., Refs. 9 and 11): it selects a particular wavenumber m in Eq. (10), produces a traveling wave and couples the neighboring spherical harmonics, such as $P_{l-2}^m(\cos\theta)e^{im\phi}$ and $P_{l+2}^m(\cos\theta)e^{im\phi}$ with the principal $P_l^m(\cos\theta)e^{im\phi}$. Third, a vital role is played by the nonlinear effect which not only maintains the differential rotation via the Reynolds stress (e.g., Refs. 16 and 20) but also alters the relative phase between the principal harmonics $P_l^m(\cos\theta)e^{im\phi}$ and the coupled ones $P_{l-2}^m(\cos\theta)e^{im\phi}$ and $P_{l+2}^m(\cos\theta)e^{im\phi}$. Consequently, a nonlinear general pattern in slowly rotating spherical or spheroidal systems with large-aspect ratios may be approximately represented by

$$\Theta=[P_l^m+\mathcal{S}P_{l-2}^m e^{i\phi_1}+(1-\mathcal{S})P_{l+2}^m e^{i\phi_2}]e^{i(m\phi+\omega t)}, \tag{11}$$

where $l\gg O(1)$, $\mathcal{S}$ is real, and ω denotes the frequency of a multiarmed spiral wave and the phase variation is introduced by ϕ_1 and ϕ_2. Note that there is a simple geometric relationship between a flattened spheroidal disk and a spherical shell in which spherical harmonics $Y_l^m(\theta,\phi)$ can be used in both spherical and spheroidal symmetries.[21] When the effect of slow rotation couples the three spherical harmonics together in Eq. (11) but without causing a relative phase change, i.e., $\phi_1=\phi_2=0$, the profile of which is shown in Fig. 3(a) for $m=2$ and $\mathcal{S}=0.34$, the multiarmed spirals cannot be formed.

By simply including a phase change, for example, $\phi_1=-2.0$ and $\phi_2=1.8$, giant two-armed spirals extending from the common core located at the rotation axis all the way to the equator are formed, as displayed in Fig. 3(b).

Despite our extensive computation over a wide range of parameters with various initial conditions at Pr=7.0, we did not find stable multiarmed spiral waves that have more than six spiral arms. As indicated in Table I, there exists slow decrease in both E_{kin} and Nu when the number of spiral arms increases. We therefore conjecture that a giant spiral structure with more than six spiral arms is nonlinearly unstable. It should be borne in mind, however, that we have not explored the effect of Pr because Pr is unlikely to play a vital role in slowly rotating, weakly nonlinear systems and because each nonlinear simulation typically takes more than 2 weeks of CPU time on a 64-processor parallel computer.

The discovery of multiarmed spiral structure in slowly rotating thin-shell systems poses a mathematically challenging problem. There exist no nonlinear mathematical theories for slowly rotating systems based on which the key properties of multiarmed spiral waves, such as the maximum number of spiral arms, can be predicted and understood. A nonlinear theory that is capable of capturing the competing effects of slow rotation and weak nonlinearity, as well as describing the secondary or higher bifurcation from a spherically symmetric state, is needed to provide a full explanation for the nonlinear multiarmed spiral waves reported in this letter.

L.L. and X.L. are supported by NSFC (Contract No. 110310773022/10633030), CAS grants, and 863-project (Grant No. 2006 AA01A125). K.H.C. is supported by Hong Kong RGC (Grant No. 700308) and K.Z. is supported by UK NERC and STFC grants. The numerical computation was supported by SSC.

[1] D. M. Elmegreen, "A near-infrared atlas of spiral galaxies," Astrophys. J., Suppl. **47**, 229 (1981).
[2] D. Barkley, "Linear stability analysis of rotating spiral waves in excitable media," Phys. Rev. Lett. **68**, 2090 (1992).
[3] E. Bodenschatz, J. R. de Bruyn, G. Ahlers, and D. S. Cannell, "Transitions between patterns in thermal convection," Phys. Rev. Lett. **67**, 3078 (1991).
[4] M. Net, I. Mercader, and E. Knobloch, "Binary fluid convection in a rotating cylinder," Phys. Fluids **7**, 1553 (1995).
[5] *Nonlinear Wave Processes in Excitable Media*, edited by A. V. Holden, M. Marcus, and H. G. Othmer (Plenum, New York, 1991).
[6] C. R. Carrigan and F. H. Busse, "An experimental and theoretical investigation of the onset of convection in rotating spherical shells," J. Fluid Mech. **126**, 287 (1983).
[7] P. A. Gilman, "Fluid dynamics and MHD of the solar convection zone and tachocline: current understanding and unsolved problems," Sol. Phys. **192**, 27 (2000).
[8] K. Zhang, "On coupling between the Poincaré equation and the heat equation: non-slip boundary condition," J. Fluid Mech. **284**, 239 (1995).
[9] C. A. Jones, A. M. Soward, and A. I. Mussa, "The onset of thermal convection in a rapidly rotating sphere," J. Fluid Mech. **405**, 157 (2000).
[10] K. Zhang, X. Liao, and F. H. Busse, "Asymptotic solutions of convection in rapidly rotating non-slip spheres," J. Fluid Mech. **578**, 371 (2007).
[11] M. Net, F. Garcia, and J. Sanchez, "On the onset of low-Prandtl-number convection in rotating spherical shells: non-slip boundary conditions," J. Fluid Mech. **601**, 317 (2008).
[12] F. Garcia, J. Sanchez, and M. Net, "Antisymmetric polar modes of thermal convection in rotating spherical fluid shells at high Taylor numbers," Phys. Rev. Lett. **101**, 194501 (2008).
[13] A. J. Chorin, "Numerical solution of the Navier–Stokes equations," Math. Comput. **22**, 745 (1968).
[14] K. Chan, L. Li, and X. Liao, "Modelling the core convection using finite element and finite difference methods," Phys. Earth Planet. Inter. **157**, 124 (2006).
[15] K. Chan, K. Zhang, L. Li, and X. Liao, "A new generation of convection-driven spherical dynamos using EBE finite element method," Phys. Earth Planet. Inter. **163**, 251 (2007).
[16] J. M. Aurnou and P. L. Olson, "Strong zonal winds from thermal convection in a rotating spherical shell," Geophys. Res. Lett. **28**, 2557, doi:10.1029/2000GL012474 (2001).
[17] F. H. Busse, "Patterns of convection in spherical shells," J. Fluid Mech. **72**, 67 (1975).
[18] P. C. Matthews, "Pattern formation on a sphere," Phys. Rev. E **67**, 036206 (2003).
[19] K. Zhang, X. Liao, and G. Schubert, "Pore water convection within carbonaceous chondrite parent bodies: Temperature-dependent viscosity and flow structure," Phys. Fluids **17**, 086602 (2005).
[20] M. Heimpel and J. Aurnou, "Turbulent convection in rapidly rotating spherical shells: A model for equatorial and high latitude jets on Jupiter and Saturn," Icarus **187**, 540 (2007).
[21] S. Lorenzani and A. Tilgner, "Fluid instabilities in precessing spheroidal cavities," J. Fluid Mech. **447**, 111 (2001).